phys. stat. sol. (a) **137**, 207 (1993)

Subject classification: 75.60

Institut für Werkstoffwissenschaften der Universität Erlangen-Nürnberg[1])

Solving Micromagnetic Problems

Towards an Optimal Numerical Method

By

D. V. BERKOV[2]), K. RAMSTÖCK, and A. HUBERT

Various possibilities to improve numerical methods for the solution of micromagnetic problems are studied. Special attention is paid to the computation of the non-local energy part – the stray field energy. The evaluation of a scalar magnetic potential using a FFT algorithm turns out to be the most powerful and reliable acceleration technique. A Landau-Lifshitz-like equation of motion is used to drive the system towards the equilibrium state, where the effective field appearing in this equation is used at the same time to calculate and monitor the system energy during the iteration process. Two classical two-dimensional micromagnetic problems in low-anisotropy materials are solved with the methods described above: the field-induced transition between asymmetric Bloch and Néel walls in a thin film, and the structure of the transition line inside an infinitely extended Bloch wall in a uniaxial material.

Verschiedene Möglichkeiten der Verbesserung der numerischen Verfahren zur Lösung mikromagnetischer Probleme werden untersucht. Der Berechnung des nicht-lokalen Energiebeitrags – der Streufeldenergie – wird dabei besondere Aufmerksamkeit gewidmet. Dabei erweist sich ein FFT-Algorithmus zur Auswertung des skalaren Potentials des Streufelds als die zuverlässigste und wirksamste Methode zur Beschleunigung der Rechnung. Eine Landau-Lifshitz-ähnliche Bewegungsgleichung wird dazu benutzt, das System in den Gleichgewichtszustand relaxieren zu lassen, wobei das dabei benutzte effektive Feld gleichzeitig dazu dient, die Gesamtenergie während des Relaxationsprozesses zu verfolgen. Das Verfahren wird an zwei klassischen zweidimensionalen mikromagnetischen Problemen erprobt, die sich auf Materialien niedriger Anisotropie beziehen: dem feldinduzierten Übergang zwischen asymmetrischen Bloch- und Néelwänden in dünnen Schichten und der Struktur der Übergangslinie innerhalb einer unendlich ausgedehnten Blochwand in einem einachsigen Material.

1. Introduction

Solving static problems in micromagnetics [1] means to find an equilibrium magnetization configuration of a ferromagnetic body by minimizing its free energy under certain conditions. Except close to the Curie temperature a ferromagnet is characterized by a constant absolute value of the local magnetic polarization vector $\boldsymbol{J}$ (in this paper we treat the terms *magnetic polarization* and *magnetization* as synonymous) which does not depend on the applied field or on the position in the magnet. This condition forms a non-linear constraint for the cartesian magnetization components: $J_x^2 + J_y^2 + J_z^2 = J_s^2$, where J_s is the spontaneous or saturation magnetization. Together with the non-local dipolar interaction between the elementary moments it leads to a rather complicated minimization problem which can be solved analytically only for a few simple cases, such as for calculating the critical field of

[1]) Martensstr. 7, W-8520 Erlangen, Federal Republic of Germany.

[2]) Permanent address: Institute of Chemical Physics, 142432 Chernogolovka, Moscow district, Russia.

magnetization reversal in uniformly magnetized ellipsoidal particles [2] or infinite cylinders [3, 4]. Therefore, the development of adequate numerical methods for the solution of such problems has attracted considerable interest in the last 25 years [5 to 30].

Still many basic aspects of constructing such algorithms are not finally settled. This is true even for the discretization geometry. In most cases a simple rectangular lattice is chosen [12, 16, 26], but others prefer an arbitrary triangular mesh [18, 22, 24]. In our view the use of a periodic lattice is virtually enforced by the long-range dipolar interaction as explained later.

The magnetic moments in a ferromagnet are coupled by the short-range quantum-mechanical exchange energy which leads to a stiffness term. The spectrum of methods for the calculation of the exchange stiffness energy ranges from the simplest Heisenberg-like expressions (the scalar product of two adjacent moments) [15] to sophisticated internode interpolation methods using a least square fit [31].

There is also no agreement concerning the best method to take into account the dipolar interaction or demagnetizing energy of a body [32]. One can find in the literature an evaluation of the demagnetizing field H_d using a dipolar approximation for non-spherical cells [11, 30], potential theory methods using a multipolar decomposition [33], indirect methods which treat the magnetic field as an independent quantity derived from a correspondingly modified functional [13, 20, 34], or "electrostatic" methods based on fictitious "magnetic charges" [6]. Several variants exist even among the charge methods depending on how the magnetic moments are interpolated. Assuming the magnetization to be constant within each cell in the discretization lattice leads to surface charges at the cell boundaries and proves adequate for high-anisotropy situations typical for hard magnetic materials. In the other extreme of low anisotropy, typical for soft magnetic materials, an improved interpolation which leads to volume instead of surface charges offers dramatic advantages by several orders of magnitude in the energy calculation accuracy for a given discretization as shown in [31].

Finally the algorithm for minimizing the micromagnetic energy is still under discussion. Frequently used are 'equation-of-motion'-type algorithms, based usually on a Landau-Lifshitz-like equation of motion for a magnetic moment in an effective field [12, 15]. Alternatively, one of the more or less standard mathematical techniques for minimizing a function of many variables is employed [19, 23], or the magnetic moments in the grid points are aligned sequentially along the effective field, updating this field after each step [6, 28].

This paper offers new approaches to some of the above-mentioned problems. In Section 2 the choice of the discretization is explained and the corresponding energy terms are written down. Section 3 introduces the effective field, and the problem of the non-local demagnetizing field evaluation is considered in detail. Our preferred method to deal with this field is based on the volume charge formulation of the stray field problem which lends itself to effective acceleration techniques and which works best together with an iteration procedure based on the Landau-Lifshits equation as explained in detail in Section 4. In Section 5 various possibilities to accelerate the algorithm are compared. Among them the fast Fourier transform (FFT) method turned out to be the most efficient one. Only a scalar FFT is needed in our version both for 2D and 3D problems. This distinguishes it from the solution presented in a recent paper [43] which applies essentially the same FFT technique on vectorial quantities.

Physical applications obtained with our algorithm are described in Section 6. We consider (i) a transition between asymmetric Bloch and asymmetric Néel walls in an external field,

and (ii) the equilibrim structure of a so-called Bloch line, the line separating two regions of opposite rotation sense within an infinitely extended Bloch wall.

2. The Continuous Formulation of Micromagnetics

According to the phenomenological theory used in micromagnetics the energy of a ferromagnetic body with a magnetization configuration $\boldsymbol{J}(\boldsymbol{r})$ can be written as a sum of several energy contributions,

$$E_{\text{tot}} = E_{\text{ext}} + E_{\text{exch}} + E_{\text{an}} + E_{\text{d}} \,. \tag{1}$$

Here E_{ext} is the energy contribution due to an external field, E_{exch} the exchange stiffness energy, E_{an} the anisotropy energy, and E_{d} the demagnetizing or stray field energy. Magnetostrictive energy terms are neglected. The effects of external stresses may be included in the effective anisotropy energy, and the effects of magnetostrictive interactions between differently magnetized domains play a role mainly in samples of macroscopic dimensions. In the dimensions characteristic for micromagnetic problems (as opposed to domain theory) these interactions are usually negligible compared to the exchange and stray field interactions.

Within the conventional continuum theory approach these energy terms can be formulated as functionals of the unit vector $\boldsymbol{m} = \boldsymbol{J}/J_{\text{s}}$ and of reduced fields $\boldsymbol{h} = \mu_0 \boldsymbol{H}/J_{\text{s}}$,

$$E_{\text{ext}} = -2K_{\text{d}} \int_V \boldsymbol{m}(\boldsymbol{r}) \cdot \boldsymbol{h}_{\text{ext}}(\boldsymbol{r}) \, \mathrm{d}V \,, \tag{1a}$$

$$E_{\text{exch}} = A \int_V [(\nabla m_x)^2 + (\nabla m_y)^2 + (\nabla m_z)^2] \, \mathrm{d}V = -A \int_V \boldsymbol{m}(\boldsymbol{r}) \cdot \Delta \boldsymbol{m}(\boldsymbol{r}) \, \mathrm{d}V \,, \tag{1b}$$

$$E_{an} = K_{\text{u}} \int_V [1 - m_x^2] \, \mathrm{d}V \,, \tag{1c}$$

$$E_{\text{d}} = -K_{\text{d}} \int_V \boldsymbol{m}(\boldsymbol{r}) \cdot \boldsymbol{h}_{\text{d}}(\boldsymbol{r}) \, \mathrm{d}V = K_{\text{d}} \int_{\Omega} \boldsymbol{h}_{\text{d}}^2(\boldsymbol{r}) \, \mathrm{d}V \,. \tag{1d}$$

Here $\boldsymbol{h}_{\text{ext}}$ is the reduced external field (which can be non-uniform), $\boldsymbol{h}_{\text{d}}$ is the demagnetizing field or stray field defined by the two conditions rot $\boldsymbol{h}_{\text{d}} = 0$ and div $\boldsymbol{h}_{\text{d}} = -\text{div}\, \boldsymbol{m}$, A is the exchange stiffness constant, K_{u} the anisotropy constant ((1c) assumes a uniaxial magnetic anisotropy along the x-axis) and K_{d} is the stray field energy constant $K_{\text{d}} = J_{\text{s}}^2/2\mu_0$ ($= 2\pi M_{\text{s}}^2$ in the Gaussian system). The integration extends either over the sample volume V or over the whole space Ω. The alternate formulations for the exchange and the stray field energies are obtained by transformations taking into account the conditions $\boldsymbol{m}^2 = 1$ and rot $\boldsymbol{h}_{\text{d}} = 0$.

The demagnetizing field can be evaluated for the given magnetization configuration (using $\Delta \boldsymbol{r} = \boldsymbol{r} - \boldsymbol{r}'$, $\boldsymbol{e} = \Delta \boldsymbol{r}/\Delta r$) by integrating over the fields of elementary dipoles,

$$\boldsymbol{h}_{\text{d}}(\boldsymbol{r}) = \int_V \frac{3\boldsymbol{e}(\boldsymbol{m}(\boldsymbol{r}') \cdot \boldsymbol{e}) - \boldsymbol{m}(\boldsymbol{r}')}{\Delta r^3} \, \mathrm{d}V' \,. \tag{2}$$

Another possibility to calculate this field uses its representation as a gradient of a scalar magnetic potential,

$$\boldsymbol{h}_{\text{d}}(\boldsymbol{r}) = -\nabla \Phi(\boldsymbol{r}) \,, \tag{3}$$

where the potential $\Phi(\boldsymbol{r})$ is derived with the tools of potential theory from the "magnetic volume charges" $\varrho(\boldsymbol{r}) = -\operatorname{div} \boldsymbol{m}(\boldsymbol{r})$ in analogy with the corresponding electrostatic problem. This formulation makes it possible to rewrite (1d) as [35]

$$E_d = K_d \int_V \varrho(\boldsymbol{r})\, \Phi(\boldsymbol{r})\, dV\,. \tag{4}$$

Magnetic surface charges ($\boldsymbol{m} \cdot \boldsymbol{n}$ at a free surface with normal $\boldsymbol{n}$, $(\boldsymbol{m}_1 - \boldsymbol{m}_2) \cdot \boldsymbol{n}$ at an interface between two material with the magnetizations $\boldsymbol{m}_1$ and $\boldsymbol{m}_2$) will also contribute to the potential Φ and to the magnetostatic energy.

To find the equilibrium magnetization distribution, the total energy (1) must be minimized with respect to the magnetization configuration under two conditions: (i) the absolute value of the magnetization is constant and equal to the saturation magnetization of the ferromagnetic body under consideration, leading in reduced units to the constraint

$$m_x^2 + m_y^2 + m_z^2 = 1\,, \tag{5}$$

and (ii) the normal derivative of the magnetization on a free surface should vanish (under the condition of zero surface anisotropy) [35],

$$\partial \boldsymbol{m}/\partial \boldsymbol{n}_\perp = 0\,. \tag{6}$$

Other boundary conditions are also possible depending on the character of the problem, such as periodic boundary conditions for the calculation of periodic stripe domains, or fixed boundary conditions for the calculation of embedded solutions within an already known environment. Also the presence of a symmetry plane in a solution may introduce special boundary conditions.

The demagnetizing energy density has a non-local character. This means that, in contrast to other energy parts, the demagnetizing energy cannot be written as a volume integral over an energy density $\varepsilon(\boldsymbol{r})$ which depends on the magnetization and its spatial derivatives at the given point $\boldsymbol{r}$ only. For example, in the two expressions (1d) and (4) used above for E_d, either the demagnetizing field $\boldsymbol{h}_d$ in (1d) or the magnetic potential Φ in (4) depend on the magnetization configuration in the whole body. This circumstance together with the non-linear restriction (5) makes the corresponding minimization problem extremely complicated, so that in practically all interesting cases a numerical solution is required.

3. The Discrete Formulation of the Problem

3.1 General considerations

The first step in a numerical approach is the discretization of the problem. One should introduce a spatial grid with N nodes with the magnetization components m_α^i, $i = 1, \ldots, N$ given at each node in this grid where the index $\alpha = 1, 2, 3$ indicates the x-, y-, and z-components. Then the demagnetizing energy can in general be expressed as a function of these magnetization components as

$$E_d = K_d \sum_{\alpha,\beta=1}^{3} \sum_{i,j=1}^{N} m_\alpha^i m_\beta^j W_{ij}^{(\alpha,\beta)}\,, \tag{7}$$

where the matrix elements $W_{ij}^{(\alpha,\beta)}$ represent the interaction energy of unit moments placed on the nodes i and j and directed along the axes α and β, respectively.

The choice of the discretization is not trivial. The usual cartesian grid, which provides the natural treatment for problems where a ferromagnetic body has the form of a rectangular prism fails to adjust to other surfaces like that of a cylinder or a sphere, causing problems to account for the corresponding boundary conditions and surface effects [20, 30]. For this reason many authors [18, 22, 24] suggest to use a tetrahedral mesh which can be generated by special computer programs [36] adjusting to arbitrary surfaces with any desired accuracy.

Unfortunately, due to the non-local character of the demagnetizing energy, practically all matrix elements $W_{ij}^{(\alpha,\beta)}$ in (7) are non-zero. They cannot be neglected even for large distances between nodes i and j because the magnetic dipole–dipole interaction has a long-range character. This means that for an arbitrary tetrahedral mesh where all cells are different and the nodes do not form a translationally invariant lattice, one must keep in memory or evaluate for each iteration all N^2 elements $W_{ij}^{(\alpha,\beta)}$, which becomes unacceptable already for a modest system with $N = 10^3$ to 10^4 elements either for computer storage capacity or computation time reasons. In a very complicated algorithm, Koehler and Fredkin [22] managed to use only $N^{4/3}$ instead of N^2 storage elements, but it appears not clear whether the stability problems associated with this approach can be controlled under all circumstances [22].

In contrast to a non-periodic grid, for a periodic cartesian grid the matrix elements $W_{ij}^{(\alpha,\beta)}$ depend only on the difference vectors $\Delta \boldsymbol{r}_{ij} = \boldsymbol{r}_i - \boldsymbol{r}_j$ between nodes i and j. Hence the interaction matrices $\boldsymbol{W}^{(\alpha,\beta)}$ have in general only $\approx N$ independent components, which makes it possible to evaluate these components only once at the beginning of the computation and store them in memory even for quite large systems with $N \approx 10^5$ nodes. Particularly in the case of soft magnetic materials most of the interesting problems relate to details within a given micromagnetic environment with no or only simple flat free surfaces, and for such problems a rectangular discretization is most adequate.

For this reason we have chosen a cartesian discretization for our algorithm. Below we consider only 2D problems, but we do not use procedures adapted to two-dimensional systems only (such as conformal mapping methods), so that a generalization of the algorithm to the 3D case is straightforward.

3.2 The discretized effective field

In general, the effective field $\boldsymbol{H}_{\text{eff}}$ acting on a given magnetic moment in a sample of volume V can be defined as a corresponding variational derivative of the energy as

$$\boldsymbol{H}_{\text{eff}} = -\frac{\delta E}{\delta \boldsymbol{J}(\boldsymbol{r})} \tag{8}$$

or

$$\boldsymbol{h}_{\text{eff}} = -\frac{1}{2VK_{\text{d}}}\frac{\delta E}{\delta \boldsymbol{m}(\boldsymbol{r})}. \tag{9}$$

In the discretized version of a problem the effective field can be defined and calculated as

$$h_{\alpha,\text{eff}}^{i} = -\frac{1}{2SK_{\text{d}}}\frac{\partial E}{\partial m_{\alpha}^{i}} \tag{10}$$

(S being the cell area in our two-dimensional problem), which gives for the external field energy this field itself. The effective field is dimensionless if the energy is understood as

energy per unit length of the infinitely long two-dimensional structure. The anisotropy and exchange fields can be found for the two-dimensional case as

$$h^i_{x,\mathrm{an}} = -Qm^i_x\,, \qquad h^i_{y,\mathrm{an}} = h^i_{z,\mathrm{an}} = 0\,, \tag{11}$$

$$h^i_{\alpha,\mathrm{exch}} = -\frac{A}{K_\mathrm{d}}\,\Delta^i m^i_\alpha \tag{12}$$

where Q is the reduced anisotropy parameter $Q = K_\mathrm{u}/K_\mathrm{d}$, and Δ^i denotes the finite difference approximation for the Laplace operator on site i. We used a five-point approximation [26, 37] to represent the second-order partial derivatives in the Laplace operator, i.e., for example,

$$\left.\frac{\partial^2 f}{\partial x^2}\right|_{x=x_i} \cong \frac{1}{12}\,\frac{-f_{i-2} + 16f_{i-1} - 30f_i + 16f_{i+1} - f_{i+2}}{(\Delta x)^2}\,. \tag{13}$$

This formula gives two orders of magnitude improvement in the accuracy of the exchange field computation at little additional expense in comparison with a three-point formula. It is directly applicable to all interior points. Depending on the boundary condition things get more involved in a certain neighbourhood of the boundaries as will be explained in the next section.

The most difficult problem is the efficient calculation of the demagnetizing contribution to the effective field. We use the magnetic potential representation (4) of the demagnetizing energy for reasons explained below. In analogy to the formulation (7) the demagnetizing energy (4) can be expressed as a quadratic form in the charges,

$$E_\mathrm{d} = K_\mathrm{d} \sum_{k,l} \varrho_k W^{(\varrho\varrho)}_{k,l} \varrho_l = K_\mathrm{d} \sum_k \varrho_k \sum_l W^{(\varrho\varrho)}_{k,l} \varrho_l = K_\mathrm{d} \sum_k \varrho_k \Phi_k\,, \tag{14a}$$

where

$$\Phi_k = \sum_l W^{(\varrho\varrho)}_{k,l} \varrho_l \tag{14b}$$

is the magnetic potential in the cell k. Here we approximate the continuous distribution of magnetic charges by constant charges inside each cell. $W^{(\varrho\varrho)}_{k,l}$ represents an interaction energy of unit volume charges ϱ placed in cells k and l, and the sums extend over all cells.

By definition of the effective field we can write (keeping in mind that only the magnetic charges depend on the magnetization):

$$h^i_{\alpha,\mathrm{d}} = -\frac{1}{2SK_\mathrm{d}}\,\frac{\partial E}{\partial m^i_\alpha} = -\sum_{k,l} W^{(\varrho\varrho)}_{k,l}\,\frac{\partial \varrho_k}{\partial m^i_\alpha}\,\varrho^{(l)} = -\sum_k \Phi_k\,\frac{\partial \varrho_k}{\partial m^i_\alpha}\,. \tag{15}$$

As discussed in the Introduction, we use volume charges as the best choice for the treatment of problems in soft magnetic materials [31]. In the simplest approximation the magnetic volume charge $\varrho = -\mathrm{div}\,\boldsymbol{m}$ averaged over one cell can be written as (see Fig. 1)

$$\varrho = -\frac{1}{2}\left[\frac{m_x^{(1,1)} + m_x^{(1,-1)} - m_x^{(-1,1)} - m_x^{(-1,-1)}}{\Delta x} + \frac{m_y^{(1,1)} + m_y^{(-1,1)} - m_y^{(1,-1)} - m_y^{(-1,-1)}}{\Delta y}\right], \tag{16}$$

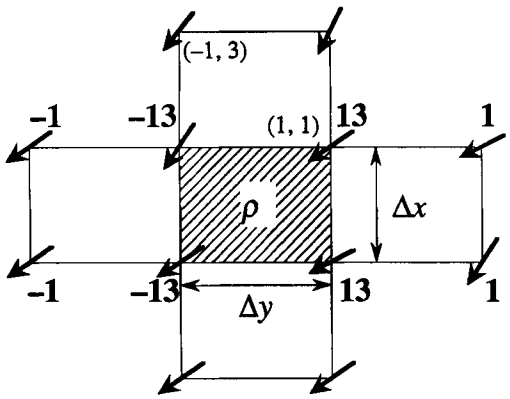

Fig. 1. The notation used for the averaged volume charge in the simple approach (16) and in the refined interpolation (18) for one cell of a rectangular lattice. The origin (0, 0) lies in the centre. The weight numbers shown in bold face apply to the x-component of the magnetization as used in (18)

where $m_x^{(1,1)}$ denotes the x-component of the magnetization in the upper right corner of the cell. Because in this approximation each charge depends on the magnetization only at the four cell corners, the derivatives in (15) are non-zero only for those four values of k for which the point $\boldsymbol{r}_i$ is a corner of the cell k.

As can be seen from (16) all derivatives with respect to an x-component of the magnetization are equal to $\pm 1/2\,\Delta x$. Inserting them into (15) one obtains the effective field on the node i in terms of magnetic potentials for those four cells which have this node as a corner,

$$h_{x,\mathrm{d}}^i = -\frac{1}{2\,\Delta x}\left(\Phi^{(1,1)} - \Phi^{(1,-1)} + \Phi^{(-1,1)} - \Phi^{(-1,-1)}\right). \tag{17}$$

We recognize that (17) represents a spatial derivative of the magnetic potential in the centre of the cell. Obviously (17) is a finite difference version of the continuous definition (3), which demonstrates that the approach is self-consistent.

Of course, for the simplest method of the magnetic charge evaluation used above, one could write down the required expression for the demagnetizing field (17) directly. But for refined evaluations of the charge from a given magnetization distribution the chosen path offers more flexibility. For example, we used a more adequate interpolation of magnetic charges based on a Lagrangian interpolation formula of the 4th order [37], which leads to a result in which the first term in (16) is replaced by

$$\frac{13(m_x^{(1,1)} + m_x^{(1,-1)} - m_x^{(-1,1)} - m_x^{(-1,-1)}) - (m_x^{(3,1)} + m_x^{(3,-1)} - m_x^{(-3,1)} - m_x^{(-3,-1)})}{12\,\Delta x}. \tag{18}$$

Test calculations have shown [31] that this representation for the magnetic charges improves the accuracy of the demagnetizing energy evaluation considerably at a negligible extra computational expense. A corresponding treatment was chosen for the surface charges.

Finally, using the definition of the effective field, the total energy can be reconstructed taking into account the degree in powers of magnetization components m_α characteristic of the different contributions to the total energy. In our case in which the anisotropy energy (1c) is a second-order expression this leads to

$$E_{\mathrm{tot}} = -K_{\mathrm{d}}\left[\sum_i \boldsymbol{m}^i \cdot \boldsymbol{h}_{\mathrm{ext}}^i + \tfrac{1}{2}\sum_i \boldsymbol{m}^i \cdot (\boldsymbol{h}_{\mathrm{an}}^i + \boldsymbol{h}_{\mathrm{exch}}^i + \boldsymbol{h}_{\mathrm{d}}^i)\right]. \tag{19}$$

For the case of a fourth-order anisotropy functional as applicable to cubic materials a coefficient of one quarter would have to be applied to the corresponding term. We found it advantageous in the process of searching for an equilibrium solution (which is to be described in the next section) to dispose of the effective field and the total energy simultaneously.

3.3 The treatment of boundaries

In this paper we limit ourselves to the simple case in which the boundaries are oriented parallel to the grid planes. In this case all variants of the boundary conditions can be treated in an elementary manner. Depending on the detailed algorithm one or more extra planes of lattice points are added outside the boundary and the magnetization values in these points are chosen according to the respective boundary condition. The limitation to simply oriented boundaries would have to be considered severe for the case of magnetic particles, but for the case of micromagnetic configurations inside soft magnetic bodies this limitation is not serious as will become apparent in the applications part of this paper.

Some care is necessary in calculating the total energy (19). The coefficients in (19) are determined by the degree of the respective energy terms in powers of the magnetization components. For the case of fixed boundary conditions where the configuration to be calculated is embedded into a given environment a coupling between variable and fixed components can lead to effectively linear contributions near the boundaries both in the exchange energy and in the stray field energy. We solved this problem by explicitly calculating an effective field $\boldsymbol{h}^*$ for which (19) is exactly fulfilled. This new field coincides with the effective field away from the boundaries and differs only near the boundaries. In the case of the demagnetizing energy the most convenient formulation was found to be one which allows for non-vanishing field contributions even on the cell boundaries and one cell distance outside them.

4. The Algorithm for the Energy Minimization

There are many algorithms to minimize the micromagnetic energy and to search for equilibrium solutions of the discretized micromagnetic equations. Even the coordinate system for the magnetization vector can be chosen in different ways. For example, in cartesian coordinates the energy is mostly a simple quadratic function of the magnetization components leading to linear equilibrium equations, but the quadratic constraint (5) converts the minimization problem into a non-linear one. On the other hand, if the magnetization is expressed in spherical coordinates, then this constraint is satisfied automatically and the number of variables per grid point is reduced from three magnetization components to two magnetization angles [27]. But in such an approach the energy is obviously non-quadratic in the angles and, in addition, a difficulty arises when moments point along the polar axis of the coordinate system, because then the azimuthal angle is ill-defined, resulting in an artificial instability in the numerical solution.

To avoid these complications we preferred the cartesian coordinate system to describe the magnetization configuration. The algorithm for the energy minimization is based on the Landau-Lifshitz equation (LLE) of motion without a precession term [16]. For each iteration step the effective field $\boldsymbol{h}^i_{\text{eff}}$ is evaluated for all nodes based on the current moment positions $\boldsymbol{m}^i_{\text{old}}$. Then for all moments simultaneously their new values are

calculated as

$$\boldsymbol{m}^i_{\text{new}} = \boldsymbol{m}^i_{\text{old}} - \alpha[\boldsymbol{m}^i_{\text{old}} \times (\boldsymbol{m}^i_{\text{old}} \times \boldsymbol{h}^i_{\text{eff}})] \,, \tag{20}$$

where $\boldsymbol{h}^i_{\text{eff}}$ denotes the effective field before the iteration is done.

The dissipation term of the LLE used in (20) effectively rotates the magnetic moment towards the effective field. By this process the absolute value of the magnetic moment is conserved up to the first order in $|\Delta \boldsymbol{m}| = |\boldsymbol{m}_{\text{new}} - \boldsymbol{m}_{\text{old}}|$, so that the condition $\boldsymbol{m}^2 = 1$ is violated only in the second order of the quantity $|\Delta \boldsymbol{m}|$ which stays small for small values of the parameter α. In a conventional gradient method the magnetization would be modified along the direction of the effective field (which points per definition opposite to the gradient), and in general this modification would strongly violate the condition $\boldsymbol{m}^2 = 1$. This means that a normalization of all moments after the iteration disturbs the configuration obtained using the LLE much less than that for an ordinary gradient method.

After the move (20) and a normalization of $\boldsymbol{m}$ we evaluate the new effective field values and the new energy E_{new}. If $E_{\text{new}} < E_{\text{old}}$, then the step is accepted and we may go on to the next iteration. If $E_{\text{new}} > E_{\text{old}}$, we restore the old moment configuration and the old values of the effective field, decrease $\alpha(\alpha \to \alpha/2)$ and try again. As long as not all effective field vectors are collinear with the magnetization vectors (which means equilibrium), we can always obtain a configuration with a smaller energy if the dissipation parameter is chosen sufficiently small.

To avoid an unnecessarily slow convergence due to too small values of α we incorporated a 'self-learning facility' in the algorithm: if some subsequent iterations are successful, the program tries to increase $\alpha(\alpha \to 2\alpha)$. Test calculations have shown that this facility provides an adequate minimization behaviour. Further refinements are being studied.

The criterion to terminate the iteration process is also based on the effective field. We assume that the equilibrium state is achieved if for all magnetic moments the absolute value of the corresponding torque fulfils the condition

$$|\boldsymbol{m}^{(i)} \times \boldsymbol{h}^{(i)}_{\text{eff}}| \leqq \varepsilon \,, \tag{21}$$

where typically a value of $\varepsilon = 10^{-4}$ was chosen. This condition assures that the component of the effective field perpendicular to the local magnetization vector is simultaneously small at all points. In this way the algorithm leads at least to a local minimum of the micromagnetic energy functional under the constraint of constant length of the magnetization vector.

In many investigations [10, 15, 16, 19] another terminating criterion is used, namely, that the relative energy difference between two subsequent iterations should be small. Criterion (21) is better for two reasons: (i) it provides local information, i.e., an information about the state of each moment, whereas in the energy criterion only a global information is available. For this reason the energy criterion can result in the termination of the iteration process when the system is still far from equilibrium, but in an almost metastable state. (ii) Another advantage of using (21) instead of the energy criterion is based on accuracy arguments. Near the minimum the energy varies only qudratically, whereas the torque varies linearly with the deviation from equilibrium. This means that the condition of zero torque can be computed more easily, while an energy criterion would need a much higher numerical accuracy to become equivalent.

5. Acceleration Techniques

The overwhelming part of the computation time for any micromagnetic algorithm is needed for the evaluation of the demagnetizing field (energy). The calculation of this field for one cell requires a summation of contributions over all other cells. In a simple algorithm we therefore need for each cell N operations (if N is the total number of cells), and for the whole system this step requires $O(N^2)$ operations. All other parts of the effective field can be evaluated using only the magnetization at the corresponding node itself plus perhaps one or two neighbour shells, which takes $O(N)$ operations per iteration for the whole body. For this reason attention should be paid first of all to the acceleration methods of the demagnetizing field evaluation.

A naive approach to the problem would be to use in the evaluation of the stray field for a given node only contributions from a few neighbours, arguing that the magnetic dipole–dipole interaction decays quite rapidly with the internode distance (as r^{-3}) [38, 39]. This idea obviously fails, because the r^{-3}-behaviour of the dipolar interaction is too weak to allow such a treatment: when the volume element $dV = r^2\, dr \ldots$ in polar coordinates is inserted into (2), the integration over the radius then obviously leads to a logarithmic expression which diverges for both large and small distances. This means that contributions from cells at all distances are equally significant and should be taken into account in a general case. Hence more sophisticated methods must be found.

5.1 The fast Fourier transform (FFT) technique

A possibility to accelerate the critical stray field part of the computation dramatically consists in applying the fast Fourier transform algorithm. This is possible because the matrix elements $W_{k,l}^{(\varrho\varrho)}$ in (14) depend only on the difference vector between the centres of cells k and l if the discretization lattice has been chosen translationally invariant. Considering for simplicity a one-dimensional system, we can write $W_{k,l}^{(\varrho\varrho)} = U_{k-l}$, and (14a) assumes the form

$$\Phi_k = \sum_l U_{k-l}\varrho_l\,, \tag{22}$$

which can be recognized as a *discrete convolution* of the functions U and ϱ.

Basically, we calculate this scalar convolution with fast Fourier transform techniques which can be done without requiring any periodicity. The first approaches to employ FFT methods in micromagnetism [41, 42] were still restricted to periodic magnetic structures. During the final stages of preparing this manuscript we learned about another paper which uses in essence the same method as the one presented here [43]. The only difference is that in [43] the Fourier transformation is applied to vectorial quantities such as the magnetization vector while our approach applies the transformation only to scalar quantities, namely the volume charge density and the potential. In two dimensions and for quadratic cells Yuan and Bertram [43] could exploit favourable symmetry properties, thus reducing the transformation to a scalar one. This seems not to be possible in three dimensions or for non-isotropic cells, however. In these cases our approach offers an advantage of a factor of two in 2D and a factor of three in 3D. In addition, our method which is detailed in the following is based on the volume charge concept which has been demonstrated to be preferable for almost stray-field-free problems [31] for other reasons.

In order to apply the Fourier transformation we remember the convolution theorem which states that the Fourier transform of the convolution of two discrete periodic functions is an element-by-element product of the Fourier transforms of the functions. In our case,

$$\tilde{\Phi}_k = \tilde{U}_k \tilde{\varrho}_k , \tag{23}$$

where $\tilde{\Phi}_k$, $\tilde{U}_k$, and $\tilde{\varrho}_k$ denote the discrete Fourier transforms of the corresponding functions,

$$\tilde{\Phi}_k = \sum_{n=0}^{N-1} e^{2\pi i k n/N} \Phi_n \quad \text{etc.} \tag{24}$$

To obtain the magnetic potential Φ_k in real space, we have to calculate the inverse Fourier transform. The demagnetizing energy can then be calculated from the potential by the simple summation (14).

The algorithm for the demagnetizing field evaluation is implemented in the following way. At the beginning of the computation the matrix of interaction coefficients U_n and the corresponding Fourier transform $\tilde{U}_k$ are evaluated once and for all. Then for each iteration the charges and their Fourier transform are calculated. Multiplying $\tilde{U}_k$ and $\tilde{\varrho}_k$, we obtain the Fourier transform of the magnetic potential $\tilde{\Phi}_k$, from which the required values Φ_n in real space are evaluated using an inverse Fourier transformation.

An actual implementation of this idea is a bit more complicated, mainly for three reasons:

(i) The functions ϱ and U are not periodic, so that we have to use the technique of 'zero padding' and to rewrite the interaction function in 'wrap-around' order [40] to satisfy all conditions of the convolution theorem. With these techniques also non-periodic problems can be handled.

(ii) For 2D or 3D a fast Fourier transformation of the corresponding dimensionality has to be applied, and the interaction function becomes a function of the difference vector between the cell position in two or three dimensions.

(iii) The interactions of the charges at the sample surface among themselves and with the volume charges have to be included. The interactions of the surface charges need considerable additional space in memory as discussed in detail in [31], but their number is smaller than the number of volume charges so that they do not contribute to the leading term in powers of the number of cells N determining the computation time in the stray field summation. It is therefore sufficient (at least in the first step) to exploit the FFT technique for the most time-consuming part, the interaction between the volume charges. The other terms may be computed by a conventional summation (although in principle the FFT technique is applicable to parts of the surface-charge-related calculations, too).

These technical details do not spoil the main advantage of the FFT that the total operation number grows with N only as $N \log(N)$ instead of N^2 which is needed otherwise for the interaction between the volume charges. We compared optimized versions of the conventional and the FFT technique for the most significant part of volume charges only. The 2D computations were performed in FORTRAN on a Hewlett Packard workstation model 720, and we obtained the following results:

1. The FFT does not introduce any additional numerical errors (as to be expected, the two methods of calculating the magnetostatic potential agree within computer accuracy).

2. The break-even point beyond which the FFT technique becomes faster was found at the very low value $N = 2^7$ ($= 8 \times 16$). For less than 128 cells the conventional summation was faster.

3. The FFT technique is ten times faster for $N = 2^{11}$ ($= 32 \times 64$) cells and already 200 times faster for $N = 2^{17}$ ($= 256 \times 512$). Only the standard FFT algorithm of [40] was used in these tests. Obviously the range of tractable problems in micromagnetism is expanded decisively due to the establishment of the FFT technique.

5.2 Variable grid methods

A fundamental problem in micromagnetics is the large range of characteristic scales in the solutions. A fine discretization which ultimately offers the highest accuracy is not very efficient in optimizing the coarse features of a configuration. We found it advantageous to start with a relatively coarse grid (say 16×32) for which an equilibrium configuration is obtained quite fast due to its modest size. The grid may then be refined in several steps. In every refinement the solution from the coarser lattice is interpolated to serve as the starting solution for the finer lattice. Convergence in the finer grids is quite fast because the configuration is already correct in its position and its coarse features. The process is repeated until the desired accuracy is achieved. Returning occasionally to a coarser lattice as is often done in numerical analysis did not offer an advantage in the cases under study. If the refinement is done by a factor of two in each step, the procedure stays fully compatible with the FFT algorithm. Comparing the total computation time required to obtain the desired accuracy using (i) the variable grid method and (ii) starting directly from the finest grid, we found that by the variable grid method an acceleration up to several times can be achieved.

5.3 Suppression of translational degeneracies

If the target configuration (such as a Bloch wall or a Bloch line) can in principle be shifted without a change in energy, this introduces unwanted uncertainties in the position of the final structure which we want to remove. We tried several methods and found the following strategy to yield optimal results: 1. In the first steps we superimposed a suitable external gradient field in order to fix the position of the micromagnetic "object" roughly. 2. After the right configuration had been formed, the gradient is switched off again, and, instead, one suitable magnetization vector is kept constant. The condition which is thus imposed onto the chosen vector must be compatible with the specific problem. All other magnetization vectors will adjust around the fixed vector. A further advantage of such a procedure is that computations with different external parameters can be immediately compared. The position of a domain wall or some other object is not left to "random" numerical influences or artifacts due to the discretization.

In reality, every domain wall which occupies a certain equilibrium position will feel an effective gradient field which favours just this position. In numerical simulation one will in general prefer to ignore these weak gradient fields in order to reduce the number of external parameters of a problem.

6. Applications

6.1 The Bloch–Néel wall transition in thin films

After the discovery of the vortex-like, almost stray-field-free domain wall configurations in thicker magnetic films [8, 44 to 46], very soon a discontinuous transition between two modes of such walls was identified as having severe consequences in the hysteretic properties

of magnetic films. Here we present a preliminary computation of the transition between the asymmetric *Bloch wall*, which is mainly stable as a 180° wall at zero field, and an asymmetric *Néel wall*, a wall type which is preferred in a field applied along the hard axis of the film in which the wall angle is reduced to values below about 150°. Both wall types are of a two-dimensional, vortex-like structure. The Bloch wall carries a single vortex with the magnetization in the centre of the wall at both surfaces opposite to each other (see Fig. 2), while the asymmetric Néel wall carries a double vortex with the central magnetization at the two surfaces displaced but parallel (and parallel to the applied field, which is the origin for the preference of this wall type in the presence of the field).

The calculation has to be considered preliminary because it ignores a well-known feature of domain walls in thin films: the extended tails which shift part of the necessary rotation particularly in Néel walls into a far outside region which certainly cannot be accommodated within a single periodic discretization lattice. Usually the range of these extended tails is several thousand times larger than the core of the wall. A multiple or variable lattice [7] is clearly necessary in order to describe properly the extended tail as well as the coupling between the tail and the core. The extended tail plays a predominant role in conventional Néel walls in very thin films. In the case of the asymmetric Néel walls in thicker films it is not unimportant [45], but suppressing it does not make the results completely meaningless. At this point we use the Bloch and Néel walls without an extended tail as a test for the procedures, postponing the complete treatment to a later date.

The present calculation applies to the following situation: An infinitely extended magnetic film of thickness D carries a uniaxial anisotropy of strength K_u with an in-plane easy axis. A domain wall is oriented along the easy axis and an in-plane magnetic field may be applied perpendicular to the easy axis. A certain range $\pm R/2$ on both sides of the wall centre is optimized in the finite element calculation. Starting from the boundaries of this range the magnetization is assumed to be fixed as determined by the equilibrium between the applied field and the uniaxial anisotropy. The wall energy is defined as the difference between the total micromagnetic energy and the energy of the uniformly magnetized domains.

The calculations were performed for the standard case of Permalloy films of 200 nm thickness. In evaporated Permalloy films as they are used in various types of thin film sensors and recording heads the material parameter $Q = K_u/K_d$ carries an extremely small value ($Q \approx 0.00025$) characteristic of a truly soft magnetic material. The detailed material and calculation parameters are included in Fig. 2.

The configuration and energy of the Bloch wall at zero field agree well with the classical result by LaBonte [6]. For the case of non-zero fields mostly Ritz method calculations based on the assumption of completely stray-field-free models were available up to now [45, 46] but see also [47]. The present results confirm the previous picture with respect to the relative stability of Bloch and Néel walls as a function of the applied field in general. They differ, however, in an interesting detail: All efforts with sophisticated test functions had led to the conclusion that the energy of the asymmetric Bloch wall increases in an applied field. The present calculation reveals that this result was an artifact which was probably due to the difficulty in describing adequately the highly asymmetric wall configurations of Bloch walls under the influence of the applied field. The energy of the asymmetric Bloch walls turns out to decrease quadratically in an applied field for all tested parameters. As a result the predicted transition field is shifted towards higher values of the applied field relative to earlier estimates, but this point may be slightly shifted back to lower fields when the extended tails are included properly in the case of the asymmetric

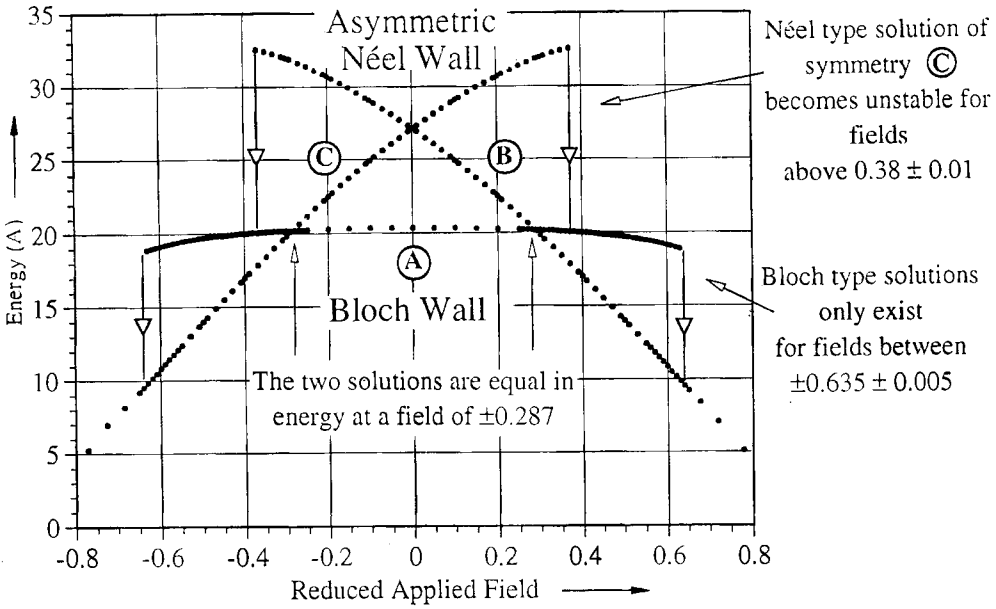

Fig. 2. The wall energy per unit wall length in units of the exchange constant A as a function of a hard axis field for a Permalloy film of 200 nm thickness and a material parameter $Q = 0.00025$. The applied field is measured in units of the anisotropy field. 128×32 discretization cells were used in this calculation. The diagram indicates both the range of absolute stability of Bloch and Néel walls as well as metastable solutions which may occur if nucleation of the more favorable wall type is inhibited. The precise range of the metastable branches may be limited by the discretization technique. Note that these results are incomplete since we neglected extended tails which are known to play a role at least in the Néel wall mode

Néel walls. The configurations found in [47] are equivalent to those found here. The critical fields will not be comparable, however, since those authors used an energy criterion together with a numerical "annealing" procedure in their iteration which max influence calculated transition fields.

In order to get an idea of the importance of the computation range R we performed calculations of the Bloch–Néel wall transition for different values of R. If R was four times larger than the film thickness D, the equal-energy point between Bloch and Néel walls was found at a reduced field of $h = 0.287$ as shown in Fig. 2. For $R/D = 8$ this break-even point was shifted to $h = 0.2845$. In comparison, an increase by a factor of four in the number of cells for a given value of R had only a negligible effect on the Bloch–Néel transition.

6.2 Transition (Bloch) lines within infinitely extended domain walls

The smooth movement of domain walls in bulk soft magnetic materials relies on their large wall width due to the small magnetocrystalline anisotropy of such materials. A necessary condition for this behaviour is, however, that the unavoidable substructures of such walls, in particular the transition lines between two wall segments of opposite rotation sense, can be moved with equal ease. The internal structure of these so-called Bloch lines is therefore of principal interest. In [48] a stray-field-free configuration of these lines was proposed, but up to now no rigorous calculation of this structure in bulk low-anisotropy materials has

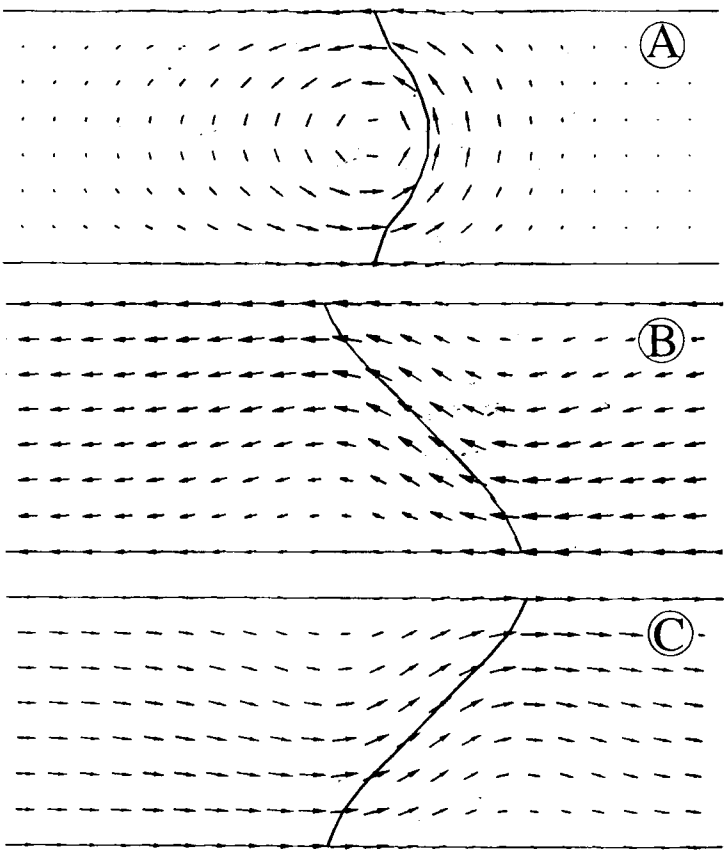

Fig. 2

been presented. We tested our algorithm on this configuration in order to try it on a situation where an unknown structure (the Bloch line) is embedded in a known non-uniformly magnetized environment (the classical Bloch or Landau wall).

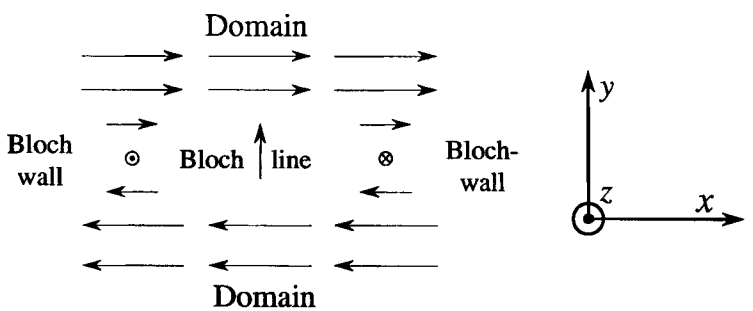

Fig. 3. The coordinate system used in the calculation of the transition line within an infinitely extended 180°-wall in a uniaxial bulk material as indicated by a cross section through the wall. The transition line is assumed to be oriented parallel to the magnetization in the centre of the undisturbed wall, that is, perpendicular to the drawing plane

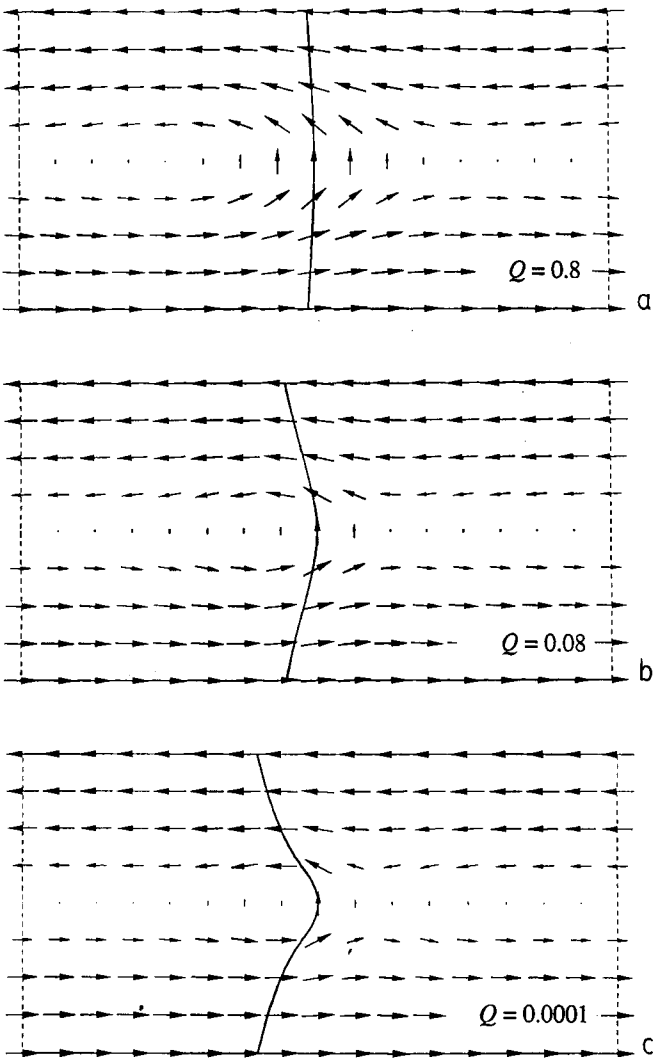

Fig. 4. Computed cross sections through Bloch lines in bulk material for three choices of the reduced anisotropy parameter Q. The example in c) corresponds closely to the stray-field-free solution proposed earlier [48], while the solution in a) is closer to 'one-dimensional' Bloch line model familiar in bubble theory. The solution was obtained with a grid of 128×64 cells, area size $24 \times 12 \sqrt{A/K_u}$. This discretization proved sufficient in the sense that no significant change in the result was observed with a refined discretization grid

In a uniaxial material with a first-order anisotropy constant K_u a 180°-domain wall is given by the following configuration (see Fig. 3):

$$m_x = \tanh\left(y/\sqrt{A/K_u}\right), \qquad m_y = 0, \qquad m_z = \pm\, 1/\cosh\left(y/\sqrt{A/K_u}\right). \tag{25}$$

The sign of the z-component of the magnetization is assumed to be positive in the left part of the wall and negative in the right part. In the domains ($|y| \to \infty$) the configuration

Table 1

The excess energies of the Bloch line in bulk uniaxial material as a function of the material parameter Q. The calculations are based on a grid with 128×64 cells, covering a total area of $24 \times 12 \sqrt{A/K_u}$. All energies are measured per unit Bloch line length in units of the exchange constant A

Q	E_{exch}	E_{dem}	E_{an}	E_{tot}
0.8000	5.618	1.726	−1.796	5.547
0.0800	9.978	1.781	−1.964	9.794
0.0080	13.093	0.787	−1.018	12.862
0.0008	14.152	0.128	−0.389	13.892
0.0001	14.034	0.023	−0.148	13.909

(25) is the same on both sides of the Bloch line. In order to be able to perform numerical calculations for the finite area limited both in x- and y-directions we create a continuous transition between the two parts of the domain wall for large but finite y by interpolating in a stray-field-free manner between the two wall modes represented by the two possible signs of m_z in (25).

We search for the lowest-energy transition between these two half-walls with opposite rotation sense but otherwise equal energy. The energy of the transition per unit length is defined as the difference between the total energy and the energy of the undisturbed Landau wall. Fig. 4 presents the resulting Bloch line configurations for different values of the anisotropy parameter Q. As predicted with the picture reproduced in [48] an almost stray-field-free, vortex-like solution is found in the limit of small Q. Not reproducible was the later type of Bloch line presented in [46] (p. 253) which was obviously due to some mysterious flaw in the computer program. Confirmed is the essential point that the width of a Bloch line in bulk soft magnetic materials is not smaller than the wall width so that

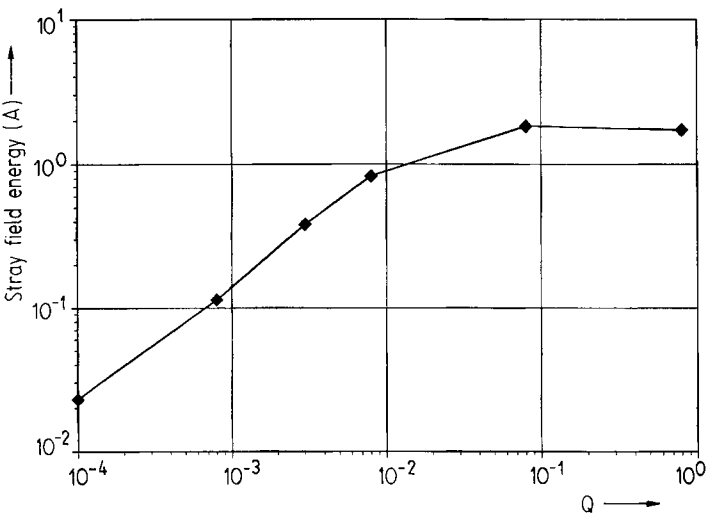

Fig. 5. The stray field energy per unit length of a Bloch line (in units of the exchange stiffness parameter A) as a function of the material parameter Q. The larger the relative importance of the demagnetizing energy, the more perfectly it is avoided

they will not interact with lattice defects in a particularly strong fashion. The total extra energy of the Bloch line and the different contributions to this excess energy are collected in Table 1.

For large Q the Bloch line loses its vortex character and assumes a more one-dimensional pattern as known from Bloch lines in bubble materials [25]. In Fig. 5 the total stray field energy of the Bloch line is plotted on a logarithmic scale as a function of the material parameter Q.

As should be expected, the stray field part of the Bloch line energy decreases with decreasing Q which means that with an increasing relative importance of the stray field energy parameter K_d over the anisotropy energy parameter K_u the actual stray field energy of the equilibrium configuration is more and more reduced. We consider the behaviour of the computed $E_d(Q)$-curve as an indication for the reliability of our algorithm at least for values of $Q > 10^{-4}$.

7. Conclusions

A micromagnetic finite element algorithm with particularly favourable properties for the computation of problems in soft magnetic materials was developed. It is based on a volume charge and scalar potential concept and on the improved interpolation scheme presented in [31]. The restriction to a periodic rectangular lattice permits the use of a scalar fast Fourier transform technique which accelerates the calculation without introducing any artifacts or any reduction in accuracy. A self-adaptive optimization of the quasi-dynamic iteration procedure led to favorable computation times. The usefulness of the algorithm was demonstrated by solving two classical two-dimensional problems: the field dependence of domain wall structures in thick magnetic films, and the structure of the Bloch line in bulk soft magnetic materials.

Acknowledgements

This work was made possible primarily by support through the CAMST program of European cooperation and a grant of the Deutsche Forschungsgemeinschaft. Thanks are due to J. Miltat, W. Sperber, and M. Dobrowolski for valuable discussions and to F. Heider and W. Andrä, sen., for critically reading the manuscript.

References

[1] W. F. BROWN, JR., Micromagnetics, John Wiley, New York 1963 (R. E. Krieger, Huntington (New York) 1978).
[2] E. C. STONER and E. P. WOHLFARTH, Phil. Trans. Roy. Soc. (London) **A240**, 599 (1948).
[3] A. AHARONI and S. SHTRIKMAN, Phys. Rev. **109**, 1522 (1958).
[4] A. AHARONI, phys. stat. sol. (a) **16**, 3 (1966).
[5] W. F. BROWN, JR. and A. E. LABONTE, J. appl. Phys. **36**, 1380 (1965).
[6] A. E. LABONTE, J. appl. Phys. **40**, 2450 (1969).
[7] R. KIRCHNER and W. DÖRING, J. appl. Phys. **39**, 855 (1968).
[8] E. DELLA TORRE, IEEE Trans. Magnetics **15**, 1225 (1979).
[9] E. DELLA TORRE, IEEE Trans. Magnetics **21**, 1423 (1985).
[10] E. DELLA TORRE, IEEE Trans. Magnetics **22**, 484 (1986).
[11] Y. D. YAN and E. DELLA TORRE, IEEE Trans. Magnetics **24**, 2368 (1988).
[12] Y. D. YAN and E. DELLA TORRE, J. appl. Phys. **66**, 320 (1989).
[13] P. ASSELIN and A. A. THIELE, IEEE Trans. Magnetics **22**, 1876 (1986).

[14] Y. NAKATANI and N. HAYASHI, IEEE Trans. Magnetics **23**, 2179 (1987).
[15] Y. NAKATANI, Y. UESAKA, and N. HAYASHI, Japan. J. appl. Phys. **28**, 2485 (1989).
[16] M. E. SCHABES and H. N. BERTRAM, J. appl. Phys. **64**, 1347 (1988).
[17] M. E. SCHABES, J. Magnetism magnetic Mater. **95**, 249 (1991).
[18] D. R. FREDKIN and T. R. KOEHLER, IEEE Trans. Magnetics **24**, 2362 (1988).
[19] D. R. FREDKIN and T. R. KOEHLER, J. appl. Phys. **63**, 3179 (1988).
[20] D. R. FREDKIN and T. R. KOEHLER, IEEE Trans. Magnetics **26**, 415 (1990).
[21] D. R. FREDKIN and T. R. KOEHLER, J. appl. Phys. **67**, 5544 (1990).
[22] T. R. KOEHLER and D. R. FREDKIN, IEEE Trans. Magnetics **28**, 1239 (1992).
[23] J. EHLERT, F. K. HÜBNER, and W. SPERBER, phys. stat. sol. (a) **106**, 239 (1988).
[24] J. EHLERT, F. K. HÜBNER, and W. SPERBER, phys. stat. sol. (a) **116**, 389 (1989).
[25] J. MILTAT, A. THIAVILLE, and P. L. TROUILLOUD, J. Magnetism magnetic Mater. **82**, 297 (1989).
[26] M. LABRUNE and J. MILTAT, IEEE Trans. Magnetics **26**, 1521 (1990).
[27] W. WILLIAMS and D. J. DUNLOP, Phys. Earth Planetary Interiors **65**, 1 (1990).
[28] J. P. JAKUBOVICS, J. appl. Phys. **69**, 4029 (1991).
[29] S. W. YUAN and H. N. BERTRAM, IEEE Trans. Magnetics **27**, 5511 (1991).
[30] D. V. BERKOV, J. Magnetism magnetic Mater. **99**, L7 (1991).
[31] K. RAMSTÖCK, T. LEIBL, and A. HUBERT, J. Magnetism magnetic Mater., to be submitted; see The CAMST Record No. 11, 4 (1992).
[32] A. AHARONI, IEEE Trans. Magnetics **27**, 3539 (1991).
[33] J. L. BLUE and M. R. SCHEINFEIN, IEEE Trans. Magnetics **27**, 4478 (1991).
[34] A. VIALLIX, F. BOILEAU, R. KLEIN, J. J. NIEZ, and P. BARAS, IEEE Trans. Magnetics **24**, 2371 (1988).
[35] L. D. LANDAU and E. M. LIFSHITZ, Electrodynamics of Continua, Pergamon Press, Oxford 1960.
[36] D. N. SHENTON and Z. J. CENDES, IEEE Trans. Magnetics **21**, 2535 (1985).
[37] M. ABRAMOVITZ and I. STEGUN, Handbook of Mathematical Functions, Dover Publ., New York 1968.
[38] J.-G. ZHU and H. N. BERTRAM, J. appl. Phys. **63**, 3248 (1988).
[39] R. H. VICTORA, Phys. Rev. Letters **58**, 1788 (1987).
[40] W. H. PRESS, P. P. FLANNERY, S. A. TENKOLSKY, and W. T. VETTERLY, Numerical Recipes. The Art of Scientific Computing (Fortran Version), Cambridge University Press, Cambridge 1989.
[41] M. MANSURIPUR and R. GILES, Computers in Phys. **4**, 291 (1990).
[42] R. C. GILES, P. R. KOTIUGA, and F. B. HUMPHREY, J. appl. Phys. **67**, 5821 (1990).
[43] S. W. YUAN and H. N. BERTRAM, IEEE Trans. Magnetics **28**, 2031 (1992).
[44] A. HUBERT, phys. stat. sol. **32**, 519 (1969).
[45] A. HUBERT, phys. stat. sol. **38**, 699 (1970).
[46] A. HUBERT, Theorie der Domänenwände in Geordneten Medien, Springer-Verlag, Berlin/Heidelberg 1974.
[47] S. W. YUAN and H. N. BERTRAM, Phys. Rev. B **44**, 12395 (1991).
[48] L. SCHÖN and U. BUCHENAU, Internat. J. Magnetism **3**, 145 (1972).

(Received February 26, 1993)